A Mechanistic Model of Uniform Hydrogen Sulfide/Carbon Dioxide Corrosion of Mild Steel

W. Sun and S. Nešić‡,***

ABSTRACT

A mechanistic model of uniform hydrogen sulfide (H_2S) and hydrogen sulfide/carbon dioxide (H_2S/CO_2) corrosion of mild steel is presented that is able to predict the rate of corrosion with time. In the model, the corrosion rate of mild steel is primarily affected by H_2S concentration, temperature, velocity, and the protectiveness of the mackinawite surface layer. The amount of mackinawite retained on the steel surface changes with time and depends on the layer formation rate as well as the layer damage rate. The layer formation may occur by corrosion and/or precipitation, while the layer damage can be by mechanical or chemical means. The model predictions were compared with a very broad set of experimental results and good agreement was found. The current version of the model does not yet include iron sulfide precipitation effects, nor hydrodynamic effects on film damage, which will be addressed in future work.

KEY WORDS: corrosion, hydrogen sulfide corrosion, kinetics, mackinawite, mechanism, mechanistic model, solid-state reaction

INTRODUCTION

Internal carbon dioxide (CO_2) corrosion of mild steel in the presence of hydrogen sulfide (H_2S) represents a significant problem for the oil and gas industry.[1-7]

In CO_2/H_2S corrosion of mild steel, both iron carbonate and iron sulfide layers can form on the steel surface. Studies have demonstrated that surface layer formation is one of the important factors governing the corrosion rate. The layer growth depends primarily on the kinetics of the layer formation. The kinetics of iron carbonate, iron sulfide, and mixed iron carbonate/sulfide layers have been quantified and reported in several recent publications by the authors' research group. These are parts of a large ongoing project focusing on modeling the internal CO_2/H_2S corrosion of mild steel.[8-9] The main operating parameters, types of equipment and measurement techniques used, and the resulting corrosion rates, for these and other similar experiments, are summarized in Table 1. However, despite the relative abundance of experimental data, the uncertain mechanism of H_2S corrosion makes it difficult to develop a model for the kinetics of iron sulfide layer formation and further to predict the corrosion rate of mild steel. Therefore, in this study, the mechanism of H_2S corrosion as well as iron sulfide formation is investigated in parallel, and a model of the overall process is proposed.

Smith and Joosten,[6] in their review paper, systematically describe much of the research work done in the area of CO_2/H_2S corrosion in the oilfield environments. It is mentioned that most of the literature is still confusing and somewhat contradictory and the mechanism of CO_2/H_2S corrosion remains unclear. The mechanisms of iron sulfide layer formation in H_2S corrosion were also reviewed by Lee.[10] In the following text, the current understanding of the mechanisms of iron sulfide layer formation will be summarized briefly.

Submitted for publication February 2008; in revised form, October 2008.

‡ Corresponding author. E-mail: nesic@ohio.edu.
* Institute for Corrosion and Multiphase Technology, Ohio University, 342 West State St., Athens, OH 45701. Present address: ExxonMobile Upstream Research Company, Houston, TX 77098.
** Institute for Corrosion and Multiphase Technology, Ohio University, 342 West State St., Athens, OH 45701.

ISSN 0010-9312 (print), 1938-159X (online)
09/000049/$5.00+$0.50/0 © 2009, NACE International

TABLE 1

Summary of the Experimental Details for All the Tests Used for Derivation of the Model (CR is Corrosion Rate, WL is Weight Loss, LPR is Linear Polarization Resistance)

Case #	T (°C)	pH_2S (bar)	pCO_2 (bar)	pH	Vel. (m/s)	Duration (h)	CR_{exp} (mm/y)	CR_{cal} (mm/y)	Equipment Measuring Technique	Ref.
1.	80	3.7E–05	0	5.5	0	24	0.1	0.21	Glass cell – WL	33
2.	80	7.4E–05	0	5.5	0	24	0.1	0.16	Glass cell – WL	33
3.	80	1.2E–04	0	5.5	0	24	0.2	0.14	Glass cell – WL	33
4.	80	2.0E–04	0	5.5	0	24	0.2	0.12	Glass cell – WL	33
5.	80	4.9E–04	0	5.5	0	1	1.5	0.43	Glass cell – WL	33
6.	80	4.9E–03	0	5.5	0	1	2.4	0.73	Glass cell – WL	33
7.	80	4.9E–02	0	5.5	0	1	3.6	2.07	Glass cell – WL	33
8.	80	4.9E–04	0	5.5	0	24	0.1	0.11	Glass cell – WL	33
9.	80	4.9E–03	0	5.5	0	24	0.1	0.15	Glass cell – WL	33
10.	80	4.9E–02	0	5.5	0	24	0.4	0.42	Glass cell – WL	33
11.	80	4.9E–04	0	5.5	0	1	1.9	0.43	Glass cell – WL	33
12.	80	4.9E–03	0	5.5	0	1	2.1	0.73	Glass cell – WL	33
13.	80	4.9E–02	0	5.5	0	1	2.8	2.07	Glass cell – WL	33
14.	80	4.9E–04	0	5.5	0	24	0.1	0.11	Glass cell – WL	33
15.	80	4.9E–03	0	5.5	0	24	0.1	0.15	Glass cell – WL	33
16.	80	4.9E–02	0	5.5	0	24	0.2	0.42	Glass cell – WL	33
17.	80	4.9E–04	0	5.5	0	1	1.5	0.43	Glass cell – WL	33
18.	80	4.9E–03	0	5.5	0	1	2.6	0.73	Glass cell – WL	33
19.	80	4.9E–02	0	5.5	0	1	2.6	2.07	Glass cell – WL	33
20.	80	4.9E–04	0	5.5	0	24	0.0	0.11	Glass cell – WL	33
21.	80	4.9E–03	0	5.5	0	24	0.3	0.15	Glass cell – WL	33
22.	80	4.9E–02	0	5.5	0	24	0.2	0.42	Glass cell – WL	33
23.	80	4.9E–02	0	5.5	0	24	0.5	0.42	Glass cell – WL	33
24.	80	4.9E–02	0	5.5	0	24	0.5	0.42	Glass cell – WL	33
25.	80	4.9E–02	0	5.5	0	24	0.5	0.42	Glass cell – WL	33
26.	80	4.9E–02	0	5.5	0	24	0.1	0.42	Glass cell – WL	33
27.	80	4.9E–02	0	5.5	0	24	0.1	0.42	Glass cell – WL	33
28.	80	4.9E–02	0	5.5	0	24	0.5	0.42	Glass cell – WL	33
29.	80	4.9E–02	0	5.5	0	24	0.2	0.42	Glass cell – WL	33
30.	80	4.9E–02	0	5.5	0	24	0.2	0.42	Glass cell – WL	33
31.	80	4.9E–02	0	5.5	0	24	0.2	0.42	Glass cell – WL	33
32.	80	4.9E–02	0	5.5	0	24	0.1	0.42	Glass cell – WL	33
33.	80	4.9E–02	0	5.5	0	24	0.1	0.42	Glass cell – WL	33
34.	80	4.9E–02	0	5.5	0	24	0.2	0.42	Glass cell – WL	33
35.	60	7.3E–03	0	5.5	0	1	1.9	0.8	Glass cell – WL	33
36.	60	7.3E–02	0	5.5	0	1	2.4	0.41	Glass cell – WL	33
37.	60	7.3E–03	0	5.5	0	24	0.3	0.17	Glass cell – WL	33
38.	60	7.3E–02	0	5.5	0	24	0.7	0.48	Glass cell – WL	33
39.	60	7.3E–03	0	5.5	0	1	2.3	0.8	Glass cell – WL	33
40.	60	7.3E–02	0	5.5	0	1	2.7	2.41	Glass cell – WL	33
41.	60	7.3E–03	0	5.5	0	24	0.2	0.17	Glass cell – WL	33
42.	60	7.3E–02	0	5.5	0	24	0.6	0.48	Glass cell – WL	33
43.	60	7.3E–03	0	5.5	0	1	1.7	0.8	Glass cell – WL	33
44.	60	7.3E–02	0	5.5	0	1	2.6	2.41	Glass cell – WL	33
45.	60	7.3E–03	0	5.5	0	24	0.2	0.17	Glass cell – WL	33
46.	60	7.3E–02	0	5.5	0	24	0.3	0.48	Glass cell – WL	33
47.	25	9.1E–03	0	5.5	0	1	1.4	0.8	Glass cell – WL	33
48.	25	9.1E–02	0	5.5	0	1	1.8	2.51	Glass cell – WL	33
49.	25	9.1E–03	0	5.5	0	24	0.1	0.16	Glass cell – WL	33
50.	25	9.1E–02	0	5.5	0	24	0.3	0.5	Glass cell – WL	33
51.	25	9.1E–03	0	5.5	0	1	1.3	0.8	Glass cell – WL	33
52.	25	9.1E–02	0	5.5	0	1	1.5	2.51	Glass cell – WL	33
53.	25	9.1E–03	0	5.5	0	24	0.1	0.16	Glass cell – WL	33
54.	25	9.1E–02	0	5.5	0	24	0.3	0.5	Glass cell – WL	33
55.	25	9.1E–03	0	5.5	0	1	1.3	0.8	Glass cell – WL	33
56.	25	9.1E–02	0	5.5	0	1	1.3	2.51	Glass cell – WL	33
57.	25	9.1E–03	0	5.5	0	24	0.2	0.16	Glass cell – WL	33
58.	25	9.1E–02	0	5.5	0	24	0.3	0.5	Glass cell – WL	33
59.	60	7.3E–03	0.80	6.6	0	1	1.9	0.87	Glass cell – WL	33
60.	60	7.3E–02	0.73	6.6	0	1	1.7	2.52	Glass cell – WL	33
61.	60	7.3E–03	0.80	6.6	0	24	0.3	0.28	Glass cell – WL	33
62.	60	7.3E–02	0.73	6.6	0	24	0.4	0.6	Glass cell – WL	33
63.	60	7.3E–03	0.80	6.6	0	1	2.0	0.87	Glass cell – WL	33
64.	60	7.3E–02	0.73	6.6	0	1	2.1	2.52	Glass cell – WL	33
65.	60	7.3E–03	0.80	6.6	0	24	0.3	0.28	Glass cell – WL	33
66.	60	7.3E–02	0.73	6.6	0	24	0.1	0.6	Glass cell – WL	33
67.	60	7.3E–03	0.80	6.6	0	1	1.8	0.87	Glass cell – WL	33
68.	60	7.3E–02	0.73	6.6	0	1	2.2	2.52	Glass cell – WL	33
69.	60	7.3E–03	0.80	6.6	0	24	0.3	0.28	Glass cell – WL	33
70.	60	7.3E–02	0.73	6.6	0	24	0.2	0.6	Glass cell – WL	33
71.	80	4.9E–04	0.53	6.6	0	1	2.1	0.34	Glass cell – WL	33
72.	80	4.9E–03	0.53	6.6	0	1	2.0	0.79	Glass cell – WL	33
73.	80	4.9E–02	0.48	6.6	0	1	2.5	2.19	Glass cell – WL	33
74.	80	4.9E–02	0.48	6.6	0	1	2.4	2.19	Glass cell – WL	33
75.	80	4.9E–04	0.53	6.6	0	24	0.2	0.19	Glass cell – WL	33

continued on next page

TABLE 1 (continued)

Summary of the Experimental Details for All the Tests Used for Derivation of the Model (CR is Corrosion Rate, WL is Weight Loss, LPR is Linear Polarization Resistance)

Case #	T (°C)	pH_2S (bar)	pCO_2 (bar)	pH	Vel. (m/s)	Duration (h)	CR_{exp} (mm/y)	CR_{cal} (mm/y)	Equipment Measuring Technique	Ref.
76.	80	4.9E–03	0.53	6.6	0	24	0.5	0.28	Glass cell – WL	33
77.	80	4.9E–02	0.48	6.6	0	24	0.2	0.54	Glass cell – WL	33
78.	80	4.9E–04	0.53	6.6	0	1	1.5	0.34	Glass cell – WL	33
79.	80	4.9E–04	0.53	6.6	0	1	2.0	0.34	Glass cell – WL	33
80.	80	4.9E–03	0.53	6.6	0	1	2.4	0.79	Glass cell – WL	33
81.	80	4.9E–02	0.48	6.6	0	1	2.8	2.19	Glass cell – WL	33
82.	80	4.9E–02	0.48	6.6	0	1	2.6	2.19	Glass cell – WL	33
83.	80	4.9E–04	0.53	6.6	0	24	0.2	0.19	Glass cell – WL	33
84.	80	4.9E–03	0.53	6.6	0	24	0.4	0.28	Glass cell – WL	33
85.	80	4.9E–02	0.48	6.6	0	24	0.2	0.54	Glass cell – WL	33
86.	80	4.9E–04	0.53	6.6	0	1	1.6	0.34	Glass cell – WL	33
87.	80	4.9E–04	0.53	6.6	0	1	1.3	0.34	Glass cell – WL	33
88.	80	4.9E–03	0.53	6.6	0	1	2.6	0.79	Glass cell – WL	33
89.	80	4.9E–02	0.48	6.6	0	1	3.3	2.19	Glass cell – WL	33
90.	80	4.9E–02	0.48	6.6	0	1	2.5	2.19	Glass cell – WL	33
91.	80	4.9E–04	0.53	6.6	0	24	0.2	0.19	Glass cell – WL	33
92.	80	4.9E–03	0.53	6.6	0	24	0.4	0.28	Glass cell – WL	33
93.	80	4.9E–02	0.48	6.6	0	24	0.2	0.54	Glass cell – WL	33
94.	80	2.0E–04	0.53	5.5	0	1	0.4	0.45	Glass cell – WL	33
95.	80	2.0E–04	0.53	5.5	2	1	2.5	0.52	Glass cell – WL	33
96.	80	2.0E–04	0.53	5.5	4	1	4.7	0.57	Glass cell – WL	33
97.	80	2.0E–04	0.53	5.5	0	20	0.2	0.12	Glass cell – WL	33
98.	80	2.0E–04	0.53	5.5	2	20	0.5	0.13	Glass cell – WL	33
99.	80	2.0E–04	0.53	5.5	4	20	0.5	0.13	Glass cell – WL	33
100.	70	0	0.00	4.2–4.9	0.3	2	7.8		Flow loop – WL	34
101.	70	0	0.00	4.2–4.9	0.3	7	8.1		Flow loop – WL	34
102.	70	0	0.00	4.2–4.9	0.3	14	7.3		Flow loop – WL	34
103.	70	0	0.00	4.2–4.9	0.3	21	7.1		Flow loop – WL	34
104.	70	0.004	137.90	4.2–4.9	0.3	2	0.4	0.8	Flow loop – WL	34
105.	70	0.004	137.90	4.2–4.9	0.3	7	0.1	0.56	Flow loop – WL	34
106.	70	0.004	137.90	4.2–4.9	0.3	14	0.1	0.48	Flow loop – WL	34
107.	70	0.004	137.90	4.2–4.9	0.3	21	0.1	0.44	Flow loop – WL	34
108.	70	0.07	137.83	4.2–4.9	0.3	2	1.2	1.92	Flow loop – WL	34
109.	70	0.07	137.83	4.2–4.9	0.3	7	0.9	1.16	Flow loop – WL	34
110.	70	0.07	137.83	4.2–4.9	0.3	14	0.2	0.9	Flow loop – WL	34
111.	70	0.07	137.83	4.2–4.9	0.3	21	0.3	0.79	Flow loop – WL	34
112.	70	0.13	137.77	4.2–4.9	0.3	2	3.7	2.5	Flow loop – WL	34
113.	70	0.13	137.77	4.2–4.9	0.3	7	1.8	1.47	Flow loop – WL	34
114.	70	0.13	137.77	4.2–4.9	0.3	14	1.0	1.12	Flow loop – WL	34
115.	70	0.13	137.77	4.2–4.9	0.3	21	1.1	0.97	Flow loop – WL	34
116.	50	8.3E–04	137.90	5	0.2	72	5.5		Flow Through – WL	5
117.	50	2.2E–03	137.90	5	0.2	72	4.7		Flow Through – WL	5
118.	50	2.9E–03	137.90	5	0.2	72	5.4		Flow Through – WL	5
119.	50	0.03944	137.86	5	0.2	72	2.1	0.62	Flow Through – WL	5
120.	50	0.05818	137.84	5	0.2	72	1.8	0.66	Flow Through – WL	5
121.	50	0.08530	137.81	5	0.2	72	2.4	0.71	Flow Through – WL	5
122.	50	0.08959	137.81	5	0.2	72	1.5	0.72	Flow Through – WL	5
123.	50	0.11653	137.78	5	0.2	72	1.9	0.76	Flow Through – WL	5
124.	20	3.8E–06	0.98	5	0.5	–	0.3	0.12	Glass cell – LPR	10
125.	20	5.1E–05	0.98	5	0.5	–	0.1	0.09	Glass cell – LPR	10
126.	20	1.3E–04	0.98	5	0.5	–	0.1	0.09	Glass cell – LPR	10
127.	20	2.3E–04	0.98	5	0.5	–	0.2	0.09	Glass cell – LPR	10
128.	120	0	0.00	4.86	10	27	30.0		Flow loop – WL	35
129.	120	1.38	6.90	4.32	10	24	1.7	3	Flow loop – WL	35
130.	120	2.76	6.90	4.09	10	20	1.8	4.34	Flow loop – WL	35
131.	120	2.76	6.90	4.09	10	138	0.9	1.89	Flow loop – WL	35
132.	120	2.76	6.90	4.09	10	166	0.8	1.73	Flow loop – WL	35
133.	120	3.45	6.90	4.01	10	22	1.9	4.57	Flow loop – WL	35
134.	120	3.45	6.90	4.01	10	383	0.7	1.26	Flow loop – WL	35
135.	120	4.14	6.90	3.95	10	69	1.4	1.26	Flow loop – WL	35
136.	60	3	0.00	—	—	71	0.8	2.06	Autoclave – WL	36
137.	60	3	0.00	—	—	91	0.5	1.81	Autoclave – WL	36
138.	70	20	0.00	—	—	91	2.9	4.26	Autoclave – WL	36
139.	65	12.2	0.00	—	—	69	1.0	3.83	Autoclave – WL	36
140.	65	8	0.00	—	—	91	1.0	2.96	Autoclave – WL	36
141.	65	4.2	0.00	—	—	63	1.3	2.44	Autoclave – WL	36
142.	80	10	6.90	3.1	1	456	0.9	1.48	Flow loop – WL	37
143.	80	10	6.90	3.1	3	456	0.9	1.48	Flow loop – WL	37
144.	80	10	6.90	3.1	5	456	1.2	1.48	Flow loop – WL	37
145.	25	10	6.90	3.2	1	504	0.6	1.19	Flow loop – WL	37
146.	25	10	6.90	3.2	3	504	1.3	1.19	Flow loop – WL	37
147.	25	10	6.90	3.2	5	504	1.0	1.19	Flow loop – WL	37
148.	80	30	6.90	2.9	1	360	1.4	2.82	Flow loop – WL	37
149.	80	30	6.90	2.9	3	360	1.1	2.82	Flow loop – WL	37
150.	80	30	6.90	2.9	5	360	1.1	2.82	Flow loop – WL	37

TABLE 2
Summary of Structural Typism in the Iron Sulfide System

Name	Formula	Structure
Amorphous	FeS	Non-crystalline
Cubic	FeS	Sphalerite-type
Troilite	FeS	Distorted niccolite-type
Mackinawite	$Fe_{1+x}S$	2D layer material
Pyrrhotite	FeS_{1+x} (or $Fe_{1-x}S$)	Distorted niccolite-type
Smythite	$Fe_{3+x}S_4$	Distorted niccolite-type
Greigite	Fe_3S_4	Thiospinel (magnetite-type)
Ferric sulfide	Fe_2S_3	Thiospinel with cation vacancies
Pyrite	FeS_2	Derived from rock salt
Marcasite	FeS_2	Isostructural with $CaCl_2$

Meyer, et al.,[11] observed that in saturated H_2S solutions, formation of a porous mackinawite layer was followed by a thicker mackinawite layer on the steel surface, which subsequently changed to pyrrhotite and pyrite.

Shoesmith, et al.,[1-2] systematically investigated the nature of iron sulfides formed on steel exposed to saturated H_2S solution at room temperature and proposed that a mackinawite layer initially formed on the steel surface by a solid-state reaction and then cracked easily. When more ferrous ions were released from the steel surface, cubic ferrous sulfide and troilite precipitated on the steel surface because of high local supersaturation of iron sulfide. If oxygen was involved in the system, formation of greigite on the steel surface was possible. At very high concentrations of H_2S, pyrrhotite, marcasite, and pyrite can form on the steel surface.

Benning, et al.,[12] reported that mackinawite was stable for four months in the reduced sulfur solutions at low temperature, and the formation rate of pyrite from a precursor mackinawite below 100°C is insignificant in the solutions at low H_2S concentration. The conversion of mackinawite to pyrite was a multistep reaction process involving changes in aqueous sulfur species, causing solid-state transformation of mackinawite to pyrite via the intermediate greigite.

Anderko and coworkers[13-16] developed a Pourbaix E-pH diagram for the multicomponent and non-ideal aqueous iron sulfide solution to predict the stability of various iron sulfide species under different conditions. The diagram indicated that the formation of iron monosulfide followed a sequence of $Fe(HS)^+$, amorphous ferrous sulfide, mackinawite, and pyrrhotite. Iron monosulfides transform to pyrite most likely through greigite and marcasite.

Smith, et al.,[3-5] proposed a model to predict the corrosion products at different H_2S concentrations and temperature in CO_2/H_2S corrosion and reported that mackinawite was the predominant species at low H_2S concentration and temperature. With the increase of H_2S concentration, mackinawite might be substituted by pyrrhotite and then pyrite. It was also suggested in their paper that the thermodynamics favored either pyrrhotite or pyrite as the corrosion products; however, the rapid kinetics of mackinawite formation favored it as the initial corrosion product. Based on the literature,[17-18] Smith and his coauthors proposed the most likely mechanism of H_2S corrosion described as follows:

—H_2S diffuses to the steel surface;
—H_2S reacts with the steel to form a mackinawite layer on the surface;
—mackinawite layer dissolves to $Fe(HS)^+$ and HS^-;
—$Fe(HS)^+$ diffuses away from the steel surface; and
—more H_2S diffuses to react with the exposed steel.

This corrosion process keeps producing a very thin "tarnish" of mackinawite, which continually forms and dissolves. Smith, et al.,[3-5] proposed this explanation for mackinawite formation and suggested that there are boundary conditions differentiating between the mackinawite corrosion product region and the other corrosion products. However, in their papers, the actual transition boundary conditions were not reported.

From the above discussion, it can be seen that many types of iron sulfides may form in H_2S environments. A summary of structural typism in the iron sulfide system are shown in Table 2.[3-5,19] However, there is no clear relationship established between the nature of the sulfide layer and the underlying corrosion process. Among those iron sulfides, mackinawite is the prevalent iron sulfide that forms on the steel surface usually as a precursor to other types of sulfides and therefore it needs to be quantified first.

The main goal of this work was to develop a practical and reasonably accurate modeling tool for oilfield situations. Therefore, while the model described below has been built up in a step-by-step manner based on mechanistic arguments, the development required a number of physically reasonable approximations, assumptions, and simplifications at various points to make progress. This was sometimes done without making a completely rigorous proof of the exact mechanistic details, guided along the most likely pathway. The closeness of the final correlation between the model and test results used for calibration will be used as the primary means to assess the validity of the assumptions and their handling, and thereby to tune and optimize the model in the future.

PHYSICO-CHEMICAL MODEL

In the literature, there seems to be a consensus that a mackinawite layer forms first on the steel surface as a product of H_2S corrosion.[1-5,17,19] In the authors' previous study,[9] mackinawite was also found to be the predominant iron sulfide species. Clearly, other types of iron sulfide layers were observed in the

past on the steel surfaces attacked by H_2S, particularly in long exposures; however, it is still unclear what effect the variation in layer composition may have on the corrosion rate.

Based on an analogy with iron carbonate formation in CO_2 solutions[8] and due to its rather low solubility, mackinawite was thought to form by a precipitation mechanism.[20] While this is clearly a possibility, as argued above, mackinawite formation via a direct heterogeneous chemical reaction with iron on the steel surface seems to be the more plausible mechanism because of the following pieces of evidence:

—Due to the very high reactivity of H_2S with iron, the mackinawite layer has been shown to form in minutes,[1-2,21] which is much faster than what one would expect from the typical kinetics for a precipitation process.[1]

—Formation of a solid mackinawite layer is observed in highly undersaturated solutions[1] (e.g., pH 3) where it is thermodynamically unstable. A case can be made that the reasoning about solubility of iron sulfide based on conditions in the bulk is invalid, since at a steel surface, due to corrosion of iron, there always exists a higher pH and a possibility to exceed the mackinawite solubility limit, even in acidic solutions. This argument would apply to even lower pH as well as to other precipitating salts such as iron carbonate. In reality, macroscopic iron carbonate layers are not observed at pH significantly below the solubility limit[22-24] (based on bulk conditions), while iron sulfide layers are.[10] In addition, basing arguments on a surface pH, which is very difficult to measure, is less practical. A way to reconcile the two arguments is to assume that upon iron dissolution, the ferrous ions never get very "far" from the steel surface due to a high local pH and rapidly form iron sulfide by precipitation. When taken to the limit, this argument amounts to a direct reaction between iron and H_2S.

—There is little effect of bulk solution supersaturation level on the rate of mackinawite formation.[20]

—The layered structure of the mackinawite layer often contains cracks and delaminations, with the steel surface imprint visible even after rather long exposures[20] (Figure 1).

—The amount of mackinawite layer always being smaller than the amount of iron lost to corrosion of mild steel (expressed in molar units)[9] and a lack of substantial mackinawite layer formation on stainless steel and other corrosion-resistant alloys (Figure 2), both suggest that the iron "source" in mackinawite is the steel itself, rather than the bulk solution.

—Mackinawite layers in corrosion tests have very similar structures and morphologies as the mackinawite layer seen in high-temperature sulfidation of mild steel exposed to gaseous or hydrocarbon environments,[25-27] where the precipitation mechanism is impossible.

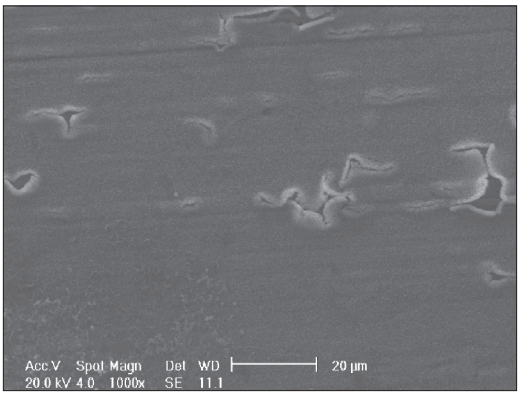

(a)

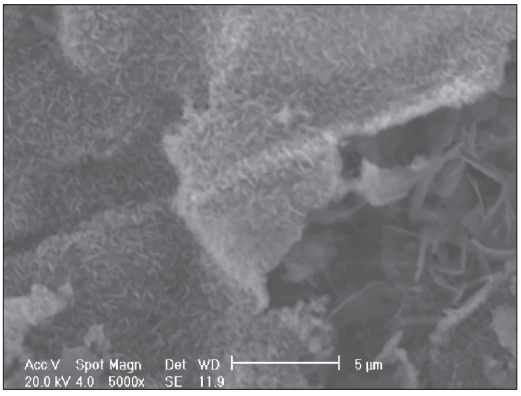

(b)

FIGURE 1. *Film morphology showing polishing marks on the X65 mild steel, (a) 1,000X and (b) 5,000X, under the conditions of total pressure p = 1 bar, 0 ppm initial Fe^{2+} aqueous concentration, 10% H_2S gas concentration, 60°C, 1 h reaction time, pH 5.0 to 5.5, and stagnant.*

If the list above is accepted as sufficient evidence, it can be concluded that the corrosion of mild steel in H_2S aqueous environments proceeds initially by a very fast, direct, heterogeneous reaction at the steel surface to form a solid adherent mackinawite layer. The overall reaction scheme can be written as:

$$Fe(s) + H_2S \Rightarrow FeS(s) + H_2 \quad (1)$$

Since the initial and final states of Fe are solid, this reaction is often referred to as the "solid-state corrosion reaction." The formed mackinawite layer may dissolve depending on the solution saturation level. For the typical pH range seen in oilfield brines (pH 4 to 7), the solution is often supersaturated with respect to iron sulfide and the mackinawite layer does not dissolve. Actually, in long exposures, iron sulfide grows by precipitation from the bulk.[28] If the pH is decreased below saturation the dissolution starts and

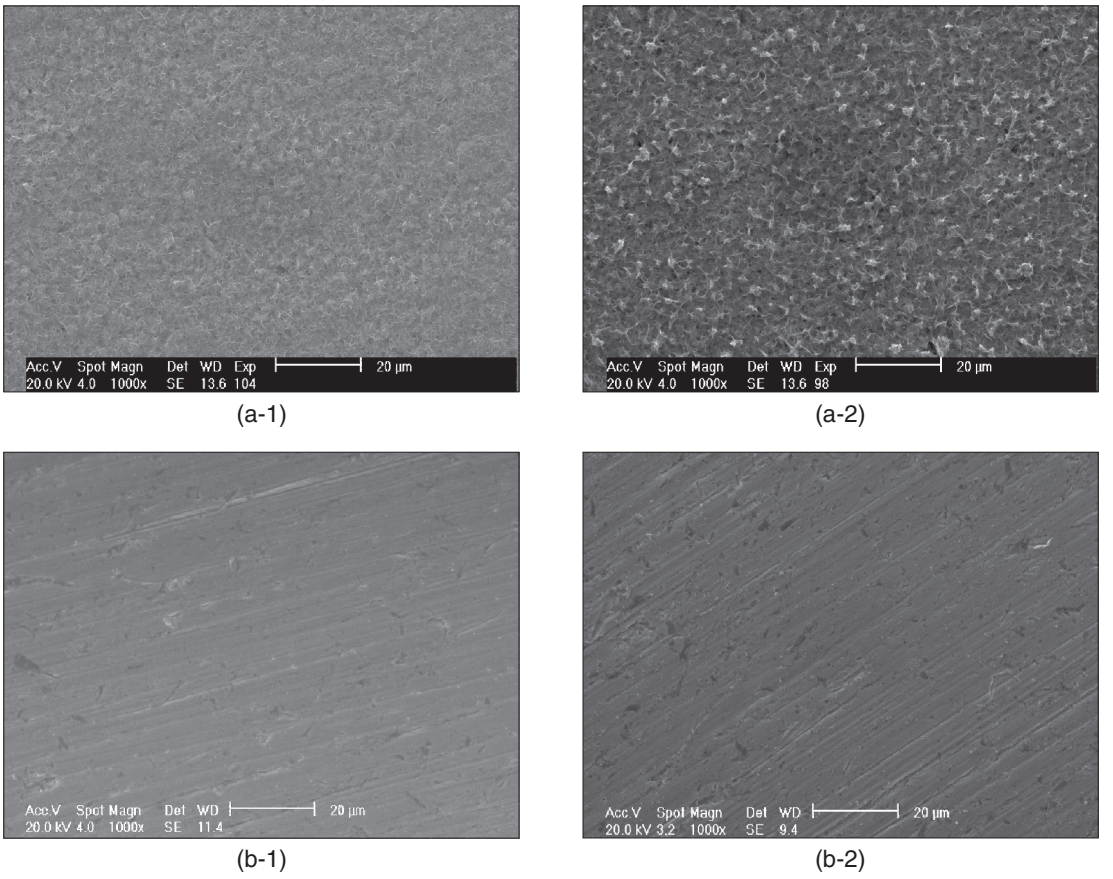

FIGURE 2. *Film morphology on the different steel surface (a-1) 0 ppm X65 mild steel Fe^{2+}, (a-2) 50 ppm X65 mild steel Fe^{2+}, (b-1) 0 ppm Type 316 stainless steel Fe^{2+}, (b-2) 50 ppm Type 316 stainless steel Fe^{2+}, under the conditions of total pressure p = 1 bar, 0.1% H_2S gas concentration, 80°C, 24 h reaction time, pH 5.0 to 5.5, and stagnant.*

the rate will increase to a point where, in the range of pH 2 to pH 3, no mackinawite can be detected on the steel surface.[1] This happens when the kinetics of mackinawite dissolution exceeds the rate formed by Reaction (1).

This first layer of mackinawite that forms very fast is extremely thin (<< 1 µm)[(1)] and invisible to the naked eye and even with a typical scanning electron microscope (SEM) or energy-dispersive spectrometer (EDS).[21] However, it is rather protective and reduces a CO_2-driven corrosion rate typically by an order of magnitude.[21]

With increased exposure times, at high H_2S concentrations and temperatures, the thin mackinawite film grows rapidly. It is still unclear whether this growth is supported by H_2S penetration through the crystalline layer (by solid-state diffusion) or if it is by ionic conduction of S^{2-}, HS^-, Fe^{2+}, etc., through the semiconductive mackinawite matrix. Outward diffusion of Fe^{2+} is consistent with an electrochemical iron dissolution mechanism and a mackinawite-continued growth at the outer film/solution interface. The inward diffusion of sulfide species is consistent with the here proposed direct reaction mechanism (Reaction [1]) and leads to mackinawite formation at the inner film interface with the steel. In both cases the mechanical integrity of the growing layer is weakened. Outward migration of Fe^{2+} leaves "voids" at the metal/mackinawite interface, i.e., it "undermines" the film that manifests itself as poor "adhesion" of the layer to the steel. Inward diffusion of the sulfide species leads to internal stresses in the layer as described below.

In the latter scenario, the solid-state corrosion Reaction (1) keeps generating mackinawite at the inner interface of the mackinawite layer with the steel. This leads to epitaxial stresses arising from the different crystalline structures of the source iron and the iron sulfide that formed in its place.[25] What is more important is that the solid iron sulfide (FeS) is calculated to be 2.56 times more voluminous than the iron it replaces at the mackinawite/steel interface. This, so-called Pilling-Bedworth ratio (PBR),[25] leads to an increase of internal compressive stresses in the mackinawite layer. When the mechanical limit of the mackinawite is exceeded, microcracking of the film occurs, thereby relieving the internal stresses and the process starts all over again. These microcracks, which most likely occur at mackinawite grain boundaries,

[(1)] It will be referred to as "mackinawite film" in the text following to distinguish it from the macroscopic outer sulfide layer.

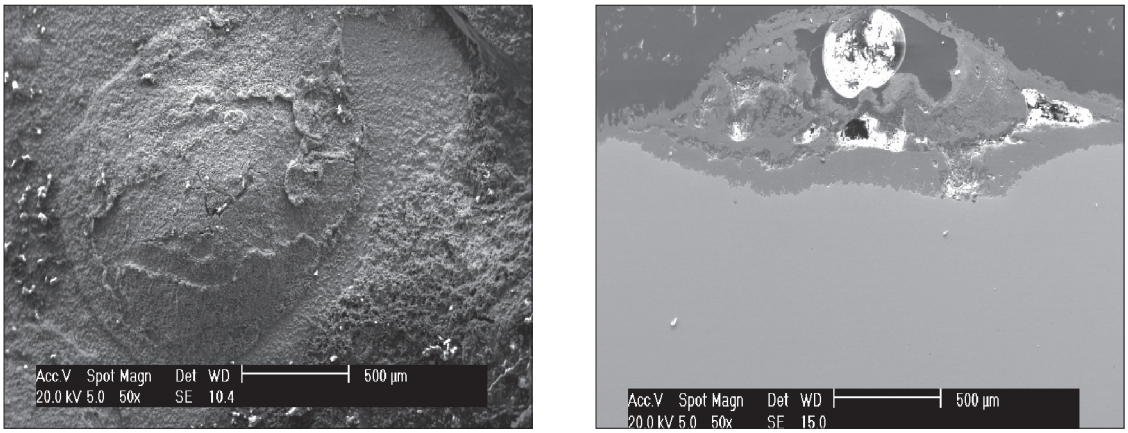

(a) (b)

FIGURE 3. *(a) Morphology and (b) cross section of the localized attack on the X65 mild steel surface in CO_2/H_2S environment under the conditions of 8 bar P_{tot}, 8 mbar PH_2S, 7.5 bar PCO_2, 60°C, and the total reaction time is 10 days.*[30]

serve as preferred pathways for a more rapid penetration of sulfide species, which fuel the solid-state Reaction (1) to go even faster.[29] It is expected that in some instances, at stress concentration points, large cracks in the film may appear as shown in Figure 1, which is confirmed to be a mackinawite film by x-ray diffraction (XRD).[9] The sulfide species penetrate even more easily at these locations to fuel the corrosion Reaction (1), which makes even more sulfide film at those locations and causes even more internal stressing and film failure. It is not difficult to see how this "feed-forward" scenario could lead to an exponential growth of the reaction rate and localized corrosion in certain locations. This scenario also offers an explanation for an apparently odd occurrence in H_2S corrosion: experimental observations indicate that pits are usually full of iron sulfide and even have a cap of sulfide, which is thicker than elsewhere on the steel surface, as shown in Figure 3 provided by Brown and Nešić.[30] This appearance is very different from the localized attack seen in CO_2 corrosion where pits are bare while the surrounding steel is covered with a protective layer. Finally, in this scenario the hydrogen atoms evolved by the corrosion Reaction (1) buildup at the steel/film interface because they can diffuse out through the tight mackinawite film only with some difficulty. This may lead to enhanced hydrogen penetration into the steel. On the other hand, the hydrogen built up at the steel/layer interface may build up pressure and "bubble out" and cause further damage to the mackinawite layer. The last few points are purely speculative and are discussed here only because they are consistent with the proposed mechanism of H_2S corrosion of steel and the resulting iron sulfide layer growth. As there is no direct evidence for them in the experiments presented in this work, these hypotheses require further evaluation in the future.

As the mackinawite layer goes through the growth/microcracking cycle, it thickens. As larger

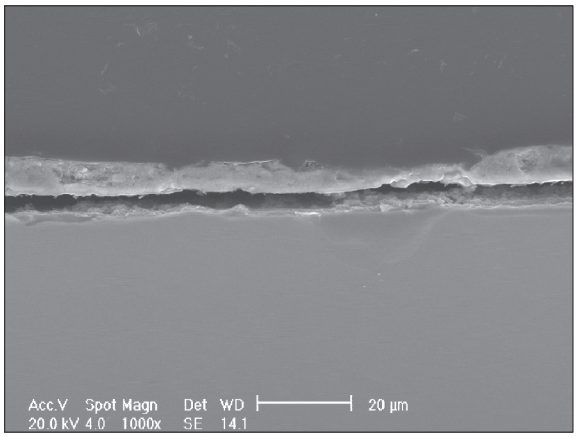

FIGURE 4. *Cross section of the layer formed on the X65 mild steel surface (at 1,000X) under the conditions of total pressure p = 1 bar, 0 ppm initial Fe^{2+} aqueous concentration, 10% H_2S gas concentration (H_2S/N_2 gas), 80°C, pH 5, and 24-h total reaction time.*

cracks appear, whole portions of the layer may partially delaminate from the steel surface starting another cycle of rapid layer growth underneath, as shown in Figure 4. Over longer exposures, this cyclic growth/delamination process leads to a macroscopically layered structure, which is rather porous. As this layer grows it will spontaneously spall, a process assisted by flow. If the bulk solution is undersaturated (typically at $3 < pH < 4$), the outer porous mackinawite layer will dissolve. This may happen even to the very tight and thin inner mackinawite film at $pH < 3$.[1]

In summary, in H_2S corrosion of mild steel, two types of mackinawite layers form on the steel surface:

—a very thin (<<1 µm) and tight inner film
—a much thicker (>>1 µm) outer layer, which is loose and very porous

The outer layer may be intermixed with any iron sulfide or iron carbonate that may have precipitated, given the favorable water chemistry and long exposure

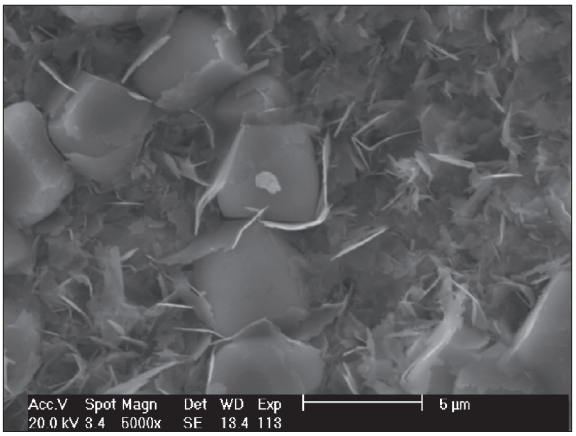

FIGURE 5. *Morphology of layer formed on the X65 mild steel surface under the conditions of 0.1% H_2S (H_2S/CO_2 gas), 80°C, pH 6.5 ~ 6.6, Fe^{2+} = 50 ppm, and 24-h total reaction time.*

time, which would change its properties and appearance. Both the inner mackinawite layer and the outer layer act as barriers for the diffusion of the sulfide species, which fuel the solid-state corrosion Reaction (1). This is in addition to the diffusion resistance through the aqueous mass-transfer boundary layer. In the authors' opinion, the hypothesis about outward diffusion by the Fe^{2+} through the thin mackinawite layer can be rejected since it is inconsistent with the proposed solid-state corrosion Reaction (1) and would lead to a formation of a very different looking and behaving sulfide layer in a process that is more akin to iron carbonate formation in CO_2 corrosion.

When CO_2 is present in the solution, both iron carbonate and iron sulfide may form on the steel surface, depending on the water chemistry as well as the competitiveness of iron carbonate and iron sulfide formation. Based on the previous investigation,[9] it is found that mackinawite layer formation is the dominant process in most cases of mixed CO_2/H_2S corrosion. In some cases, iron carbonate crystals may form intermixed with the mackinawite layer (for an example see Figure 5 [experiment with 0.1% H_2S, Fe^{2+} 50 ppm, and 80°C]), which was confirmed using XRD (Figure 6). However, the first mackinawite layer is assembled extremely quickly by a solid-state reaction; hence, it always forms first on the steel surface. The iron carbonate crystals may precipitate in the outer part of the mackinawite layer according to the crystal morphology, as shown in Figure 5. Therefore, it is believed that in mixed CO_2/H_2S systems, the mackinawite layer still partially protects the steel from corrosion, and the description of the H_2S corrosion process presented above for pure H_2S corrosion is also applicable for CO_2/H_2S corrosion, with small modifications. The assumptions that iron carbonate layer formation has little effect on the CO_2/H_2S corrosion process is a simplification; however, it does allow development of a practical working model.

MATHEMATICAL MODEL

H_2S Corrosion

Based on the experimental results and the description of the H_2S corrosion process presented above, a mathematical model can be constructed. The key assumptions are:

—the corrosion process happens via a direct heterogeneous solid-state Reaction (1) at the steel surface;

—there is always a very thin (<<1 µm) but dense film of mackinawite at the steel surface, which acts as a solid-state diffusion barrier for the sulfide species involved in the corrosion reaction;

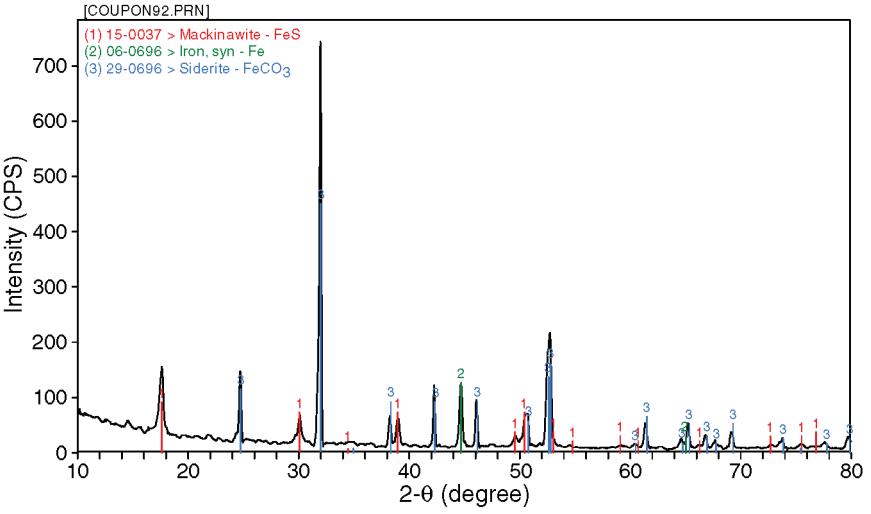

FIGURE 6. *XRD results of layer formed on the X65 mild steel surface under the conditions of 0.1% H_2S (H_2S/CO_2 gas), 80°C, pH 6.5 ~ 6.6, Fe^{2+} = 50 ppm, and 24-h total reaction time.*

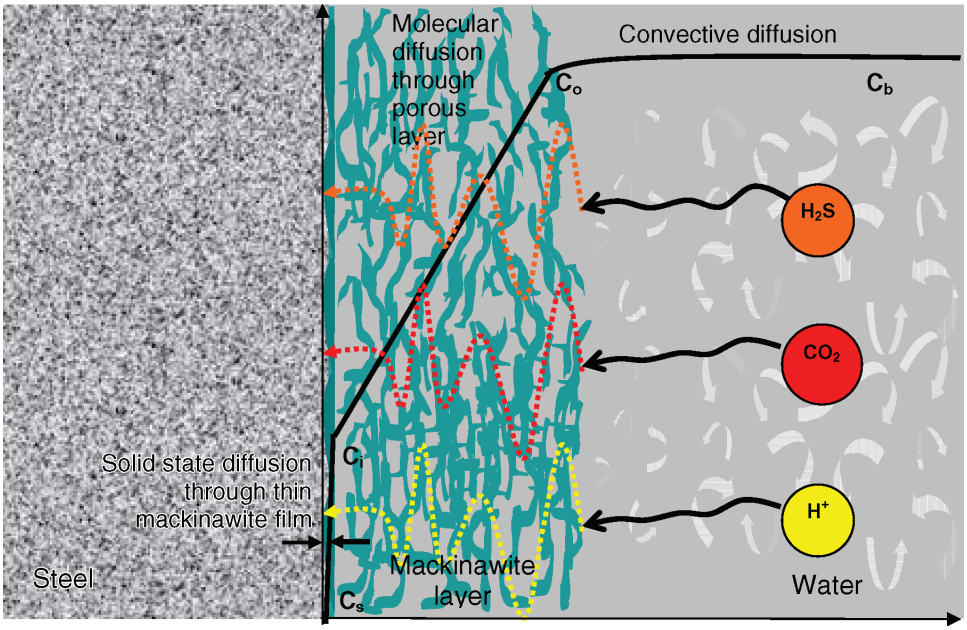

FIGURE 7. *Schematic of the H_2S corrosion process.*

—this film continuously goes through a cyclic process of growth, cracking, and delamination, which generates the outer mackinawite layer;
—this outer layer grows in thickness (typically >1 μm) over time and presents a diffusion barrier;
—the outer layer is very porous and rather loosely attached; over time it cracks, peels, and spalls, a process aggravated by the flow.

Due to the presence of the inner mackinawite film and the porous outer layer (if present), it is assumed that the corrosion rate of steel in H_2S solutions is always under mass-transfer control rather than electrochemical or chemical kinetics control. Based on the discussions above, a schematic of the H_2S corrosion process is shown in Figure 7. Based on this depiction, one can write the flux of H_2S as a result of:

—convective diffusion through the mass-transfer boundary layer:

$$Flux_{H_2S} = k_{m,H_2S}\left(c_{b,H_2S} - c_{o,H_2S}\right) \quad (2)$$

—molecular diffusion through the liquid in the porous outer layer:

$$Flux_{H_2S} = \frac{D_{H_2S}\varepsilon\Psi}{\delta_{os}}\left(c_{o,H_2S} - c_{i,H_2S}\right) \quad (3)$$

—solid-state diffusion through the inner mackinawite film:

$$Flux_{H_2S} = A_{H_2S}\ln\left(\frac{c_{i,H_2S}}{c_{s,H_2S}}\right) \quad (4)$$

where:
$Flux_{H_2S}$: flux of H_2S expressed in mol/(m^{2}s)
k_{m,H_2S}: mass-transfer coefficient for H_2S in the hydrodynamic boundary layer, $k_{m,H_2S} = 1.00 \times 10^{-4}$ in nearly stagnant conditions, in m/s
c_{b,H_2S}: bulk concentration of H_2S in the liquid phase in mol/m^3
c_{o,H_2S}: interfacial concentration of H_2S at the outer layer/solution interface in mol/m^3
D_{H_2S}: diffusion coefficient for dissolved H_2S in water, $D_{H_2S} = 2.00 \times 10^{-9}$, in m^2/s
ε: outer mackinawite layer porosity
Ψ: outer mackinawite layer tortuosity factor
c_{i,H_2S}: interfacial concentration of H_2S at the inner layer/film interface in mol/m^3
δ_{os}: thickness of the mackinawite layer, $\delta_{os} = m_{os}/(\rho_{FeS} A)$, in m
m_{os}: mass of the mackinawite layer in kg
A: surface area of the steel in m^2
A_{H_2S}: solid-state diffusion kinetic constant for H_2S: $A_{H_2S} = 2.0 \times 10^{-5}$ mol/(m^{2}s)
T_k: temperature in K
c_{s,H_2S}: "near-zero" concentration of H_2S on the steel surface set to 1.00×10^{-7} in mol/m^3

In a steady state, the three fluxes are equal to each other and are equivalent to the corrosion rate: $CR_{H_2S} = Flux_{H_2S}M_{Fe}/\rho_{Fe}$ (further corrected for appropriate corrosion rate unit mm/y or mpy), where M_{Fe} is the molecular mass of Fe and ρ_{Fe} is the density of Fe. By eliminating the unknown interfacial concentrations c_{o,H_2S} and c_{i,H_2S} from Equations (2) through (4), the following equation is obtained for the flux (corrosion rate) due to H_2S:

$$\mathrm{Flux}_{H_2S} = A_{H_2S} \ln \frac{c_{b,H_2S} - \mathrm{Flux}_{H_2S}\left(\frac{\delta_{0.5}}{D_{H_2S}\varepsilon\Psi} + \frac{1}{k_{m,H_2S}}\right)}{c_{s,H_2S}} \quad (5)$$

This is an algebraic, nonlinear equation with respect to Flux_{H_2S}, which does not have an explicit solution but can be solved by using a simple, numerical algorithm such as the interval halving method or similar. These are available as ready-made routines in spreadsheet applications or in any common computer programming language. The prediction for Flux_{H_2S} depends on a number of constants used in the model that can be found in handbooks (such as D_{H_2S}), calculated from the established theory (e.g., k_{m,H_2S}), or are determined from experiments (e.g., A_{H_2S}, c_{s,H_2S}). The unknown thickness of the outer sulfide layer changes with time and needs to be calculated as described below.

It is assumed that the amount of layer retained on the metal surface at any point in time depends on the balance of:

—layer formation kinetics (because the layer is generated by spalling of the thin mackinawite film underneath it and by precipitation from the solution), and

—layer damage kinetics (because the layer is damaged by intrinsic or hydrodynamic stresses and/or by chemical dissolution).

$$\underbrace{\mathrm{SRR}}_{\substack{\text{sulfide layer}\\ \text{retention}\\ \text{rate}}} = \underbrace{\mathrm{SFR}}_{\substack{\text{sulfide layer}\\ \text{formation}\\ \text{rate}}} - \underbrace{\mathrm{SDR}}_{\substack{\text{sulfide layer}\\ \text{damage}\\ \text{rate}}} \quad (6)$$

where all the terms are expressed in mol/(m^2s). It is assumed here that in the typical range of application (4 < pH < 7), precipitation and dissolution of the iron sulfide layer do not play a significant role, so it can be written:

$$\underbrace{\mathrm{SRR}}_{\substack{\text{sulfide layer}\\ \text{retention}\\ \text{rate}}} = \underbrace{\mathrm{CR}}_{\substack{\text{corrosion}\\ \text{rate}}} - \underbrace{\mathrm{SDR_m}}_{\substack{\text{sulfide layer}\\ \text{mechanical}\\ \text{damage rate}}} \quad (7)$$

Experiments[9] have shown that even in stagnant conditions about half of the sulfide layer that forms is lost from the steel surface due to intrinsic growth stresses by internal cracking and spalling, i.e.:

$$\mathrm{SDR_m} \approx 0.5\ \mathrm{CR} \quad (8)$$

More experimentation is required to determine how the mechanical layer damage is affected by hydrodynamic forces.

Once the layer retention rate SRR is known, the change in mass of the outer sulfide layer can easily be calculated as:

$$\Delta m_{os} = \mathrm{SRR}\ M_{FeS}\ A\ \Delta t \quad (9)$$

where M_{FeS} is the molar mass of iron sulfide in kg/mol and Δt is the time interval in seconds. The porosity of the outer mackinawite layer was determined to be very high ($\varepsilon \approx 0.9$) by comparing the weight of the layer with the cross-sectional SEM images showing its thickness. On the other hand, this layer has proven to be rather protective (i.e., impermeable to diffusion), which can only be explained by its low tortuosity arising from its layered structure. By matching the measured and calculated corrosion rates in the presence of the outer mackinawite layer, the tortuosity factor was calculated to be $\Psi = 0.003$.

A time-marching explicit solution procedure could now be established where:

—the corrosion rate Flux_{H_2S} in the absence of the outer sulfide layer can be calculated by using Equation (5), and assuming $\delta_{os} = 0$;

—the amount of sulfide layer Δm_{os} formed over a time interval Δt is calculated by using Equation (9);

—the new corrosion rate Flux_{H_2S} in the presence of the sulfide layer can be recalculated by using Equation (5);

—a new time interval Δt is set and the second and third steps are repeated.

Effect of pH

A small complication arises from the fact that at very low H_2S gas concentrations (ppm_w range), there is very little dissolved H_2S and the corrosion rate is directly affected by pH. A mackinawite layer still forms and controls the corrosion rate; however, the corrosion process is largely driven by the reduction of protons, rather than of H_2S (the case shown in Reaction [1]). In an analogy with the approach laid out above, the convective diffusion flux of protons through the mass-transfer boundary layer is:

$$\mathrm{Flux}_{H^+} = k_{m,H^+}\left(c_{b,H^+} - c_{o,H^+}\right) \quad (10)$$

which in a steady state is equal to the diffusion flux of protons through the pores of the iron sulfide layer:

$$\mathrm{Flux}_{H^+} = \frac{D_{H^+}\varepsilon\Psi}{\delta_{oc}}\left(c_{o,H^+} - c_{i,H^+}\right) \quad (11)$$

which is equal to the solid-state diffusion flux of protons through the thin mackinawite film:

$$\mathrm{Flux}_{H^+} = A_{H^+} \ln\left(\frac{c_{i,H^+}}{c_{s,H^+}}\right) \quad (12)$$

which is equivalent to the corrosion rate by protons: $CR_{H^+} = \frac{\mathrm{Flux}_{H^+}}{2}\frac{M_{Fe}}{\rho_{Fe}}$ (further corrected for the appropriate corrosion rate unit).

By eliminating the unknown interfacial concentrations c_{o,H^+} and c_{i,H^+} from Equations (10) through (12), the following expression is obtained for the flux of protons controlled by the presence of the iron sulfide layers:

$$Flux_{H^+} = A_{H^+} \ln \frac{c_{b,H^+} - Flux_{H^+}\left(\frac{\delta_{0.5}}{D_{H^+}\varepsilon\Psi} + \frac{1}{k_{m,H^+}}\right)}{c_{s,H^+}} \quad (13)$$

where:

$Flux_{H^+}$: flux of protons expressed in mol/(m²s)
k_{m,H^+}: mass-transfer coefficient for protons in the hydrodynamic boundary layer, $k_{m,H^+} = 3.00 \times 10^{-4}$ in nearly stagnant condition, in m/s
c_{b,H^+}: bulk concentration of H^+ in the liquid phase in mol/m³
c_{o,H^+}: interfacial concentration of H^+ at the outer layer/solution interface in mol/m³
D_{H^+}: diffusion coefficient for dissolved H^+ in water, $D_{H^+} = 2.80 \times 10^{-8}$, in m²/s
c_{i,H^+}: interfacial concentration of H^+ at the inner layer/film interface in mol/m³
A_{H^+}: solid-state diffusion kinetic constant for H^+: $A_{H^+} = 4.0 \times 10^{-4}$ mol/(m²s)
c_{s,H^+}: "near-zero" concentration of H^+ on the steel surface set to 1.00×10^{-7} in mol/m³

The total rate of corrosion in this case is equal to the sum of the corrosion caused by H_2S and the corrosion caused by H^+:

$$Cr = CR_{H_2S} + CR_{H^+} \quad (14)$$

This description completes the explanation of a basic mechanistic model of pure H_2S corrosion of mild steel. Based on the present model, a similar expression is proposed for combined CO_2/H_2S corrosion below.

Effect of CO_2

In the case of mixed H_2S/CO_2 corrosion, the mass-transfer-limited flux of CO_2 can be calculated from the:

—convective diffusion of CO_2 through the mass-transfer boundary layer:

$$Flux_{CO_2} = k_{m,CO_2}\left(c_{b,CO_2} - c_{o,CO_2}\right) \quad (15)$$

—molecular diffusion of CO_2 through the liquid in the porous outer sulfide layer:

$$Flux_{CO_2} = \frac{D_{CO_2}\varepsilon\Psi}{\delta_{0.5}}\left(c_{o,CO_2} - c_{i,CO_2}\right) \quad (16)$$

—solid-state diffusion of CO_2 through the inner mackinawite film:

$$Flux_{CO_2} = A_{CO_2} \ln\left(\frac{c_{i,CO_2}}{c_{s,CO_2}}\right) \quad (17)$$

which is equivalent to the corrosion rate by CO_2: $CR_{CO_2} = Flux_{CO_2} M_{Fe}/\rho_{Fe}$ (further corrected for appropriate corrosion rate unit).

By eliminating the unknown interfacial concentrations c_{o,CO_2} and c_{i,CO_2}, from Equations (15) through (17), the following expression is obtained for the corrosion rate driven by the presence of CO_2 and controlled by the presence of the iron sulfide layers:

$$Flux_{CO_2} = A_{CO_2} \ln \frac{c_{b,CO_2} - Flux_{CO_2}\left(\frac{\delta_{0.5}}{D_{CO_2}\varepsilon\Psi} + \frac{1}{k_{m,CO_2}}\right)}{c_{s,CO_2}} \quad (18)$$

where:

$Flux_{CO_2}$: flux of CO_2 expressed in mol/(m²s)
k_{m,CO_2}: mass-transfer coefficient for CO_2 in the hydrodynamic boundary layer, $k_{m,CO_2} = 1.00 \times 10^{-4}$ in nearly stagnant conditions, in m/s
c_{b,CO_2}: bulk concentration of CO_2 in the liquid phase in mol/m³
c_{o,CO_2}: interfacial concentration of CO_2 at the outer layer/solution interface in mol/m³
D_{CO_2}: diffusion coefficient for dissolved CO_2 in water, $D_{CO_2} = 1.96 \times 10^{-9}$, in m²/s
c_{i,CO_2}: interfacial concentration of CO_2 at the inner layer/film interface in mol/m³
A_{CO_2}: solid-state diffusion kinetic constant for CO_2: $A_{CO_2} = 2.0 \times 10^{-6}$ mol/(m²s)
c_{s,CO_2}: concentration of CO_2 on the steel surface in mol/m³

In the H_2S corrosion model presented above, pure mass-transfer control is assumed, and hence, the c_{s,H_2S} and c_{s,H^+} are set to be virtually zero (practically a very small value of 1.00×10^{-7} mol/m³). In CO_2 corrosion, it is the carbonic acid (H_2CO_3) that is the corrosive species, and one must account for the fact that the CO_2 hydration step-forming H_2CO_3 at the steel surface is a slow rate-controlling process. Therefore, the CO_2 flux can be equated to the limiting rate of H_2CO_3 hydration at the steel surface as follows:[31]

$$Flux_{CO_2} = c_{s,CO_2}\left(D_{H_2CO_3}\varepsilon\Psi k^f_{hyd} K_{hyd}\right)^{0.5} \quad (19)$$

where:

$D_{H_2CO_3}$: diffusion coefficient of H_2CO_3 in m²/s
K_{hyd}: equilibrium constant for the CO_2 hydration reaction
k^f_{hyd}: forward reaction rate for the CO_2 hydration reaction

By eliminating c_{s,CO_2} from Equations (18) and (19), the CO_2 flux equation takes its final form:

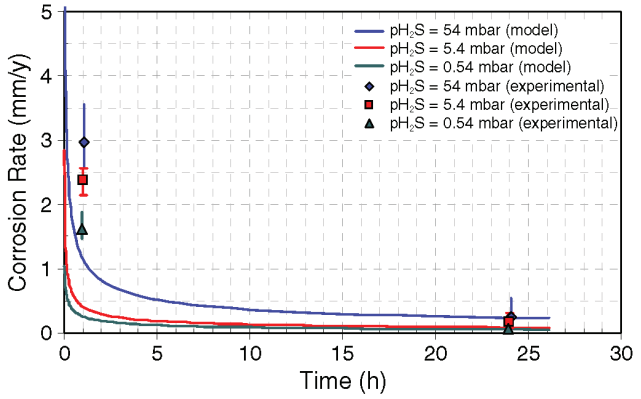

FIGURE 8. *Corrosion rate vs. time; experimental data = points, model predictions = lines; conditions: total pressure p = 1 bar, H_2S gas partial pressure from 0.54 mbar to 54 mbar, 80°C, experiment duration 1 h to 24 h, pH 5.0 to 5.5, stagnant. Experimental data taken from Sun.*[33]

$$Flux_{CO_2} = A_{CO_2} \ln \frac{c_{b,CO_2} - Flux_{CO_2}\left(\frac{\delta_{0.5}}{D_{CO_2}\varepsilon\Psi} + \frac{1}{k_{m,CO_2}}\right)}{\frac{Flux_{CO_2}}{\left(D_{H_2CO_3}\varepsilon\Psi k^{f}_{hyd} K_{hyd}\right)}} \quad (20)$$

The bulk concentration of CO_2, c_{b,CO_2}, can be obtained via Henry's law:

$$c_{b,CO_2} = P_{CO_2} \quad K_{sol} \quad (21)$$

where Henry's constant is a function of temperature and ionic strength:

$$K_{sol} = \frac{14.5}{1.00258} \quad 10^{-\left(2.27+5.65\ 10^{-3} T_f - 8.06\ 10^{-6} T_f^2 + 0.075\ I\right)} \quad (22)[32]$$

T_f is the temperature in °F and I is the ionic strength in mol/L.

By solving the above equation, the CO_2 corrosion rate can be obtained and introduced into Equation (23) below to obtain the total corrosion rate in mixed CO_2/H_2S environments:

$$CR = CR_{H_2S} + CR_{H^+} + CR_{CO_2} \quad (23)$$

For the corrosion rates caused by H_2S and H^+, the same expressions can be used as presented above for a CO_2-free environment, Equations (5) and (13), respectively.

VERIFICATION AND TESTING OF THE MODEL

Experiments by Sun[33]

To formulate the model and calibrate its performance, the experimental findings of Sun[33] were used as the primary source. Figure 8 shows the comparison of the corrosion rate vs. the reaction time for a series of pure H_2S experiments (pH_2S = 0.5 mbar to 50 mbar) done at pH 5 and 80°C, conducted by Sun.[33] Clearly, the model successfully captures the rapid reduction of the corrosion rate with time due to the growth of an iron sulfide layer. While an attempt was made to capture the very short-term data (obtained after 1 h of exposure), this was not always accurate and the main effort was directed to predicting the 24-h data points accurately. From Figure 8, one can observe that H_2S partial pressure plays an important role in corrosion. At pH_2S = 50 mbar, H_2S is the main corrosive species (contributing 98% to the overall corrosion damage when compared to only 2% attributed to H^+). When the amount of H_2S is reduced 100 times (pH_2S = 0.5 mbar), both species are responsible for approximately one half of the observed corrosion rate. Figure 9 shows the comparison of the measured and predicted amount of iron sulfide, which is retained on the steel surface at different reaction times. The predicted layer growth is very rapid in the first few hours and then gradually levels off, leading to what is often referred to as a "parabolic film growth regime."

Data were also collected by Sun[33] under rather similar conditions, with the main difference being a higher pH 6.6 and the presence of CO_2. The comparison between measured and predicted corrosion rate in this mixed H_2S/CO_2 corrosion environment is shown in Figure 10. Very similar trends are observed with time at different pH_2S, as was the case for a pure H_2S environment. Upon closer inspection of the predictions, it is found that at a pCO_2/pH_2S ratio of 10^3 in the gas phase (pCO_2 = 0.54 bar, pH_2S = 0.54 mbar), the main corrosive species is CO_2 (i.e., H_2CO_3) as expected, which is responsible for more than 90% of the corrosion rate. However, under these conditions the corrosion rate is still controlled by the presence of H_2S, i.e., sulfide layer, which reduces the pure CO_2 (H_2S-free) corrosion rate by more than 10 times. When the pCO_2/pH_2S ratio in the gas is reduced to 10, both corrosive gases contribute approximately the same to the overall corrosion rate.

The model was tested further by making simulations outside the range of parameters used to calibrate it (taken from the experimental study of Sun[33] mentioned above); i.e., the model was used to extrapolate the corrosion rates to much lower and much higher partial pressures of H_2S as well as much longer exposure times.

Experiments by Singer, et al.[34]

A similar range of H_2S partial pressures, as reported by Sun,[33] was investigated by Singer, et al.[34] The key difference was the higher partial pressure of CO_2 (pCO_2 = 2 bar) and more importantly the long duration of experiments (21 days) conducted in stratified gas-liquid pipe flow. The comparison of the model predictions and the experimental results is given in

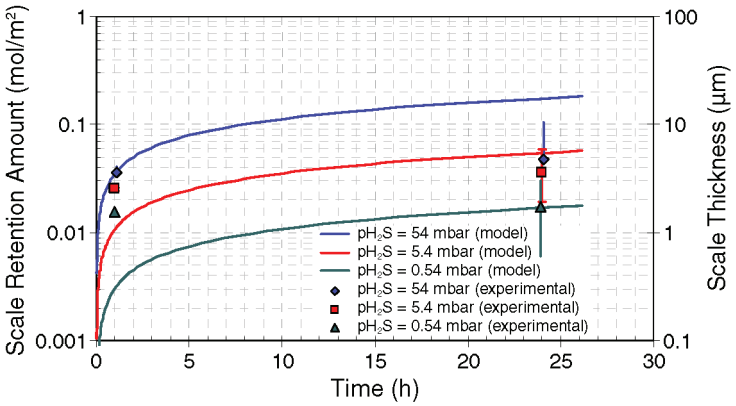

FIGURE 9. *Scale retention amount vs. time; experimental data = points, model predictions = lines; conditions: total pressure p = 1 bar, H_2S gas partial pressure from 0.54 mbar to 54 mbar, 80°C, experiment duration 1 h to 24 h, pH 5.0 to 5.5, stagnant. Experimental data taken from Sun.*[33]

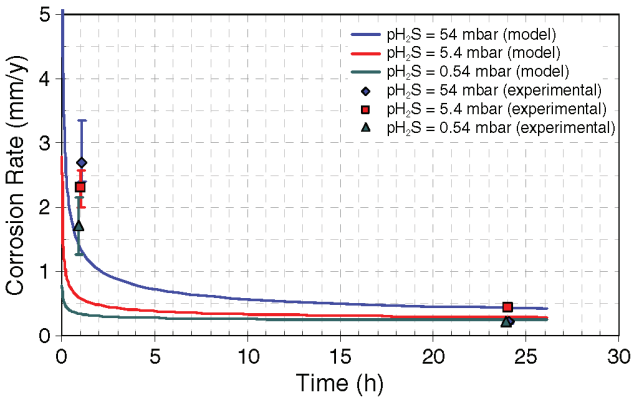

FIGURE 10. *Corrosion rate vs. time; experimental data = points, model predictions = lines; conditions: total pressure p = 1 bar, CO_2 partial pressure 0.54 bar, H_2S gas partial pressure from 0.54 mbar to 54 mbar, 80°C, experiment duration 1 h to 24 h, pH 6.6, stagnant. Experimental data taken from Sun.*[33]

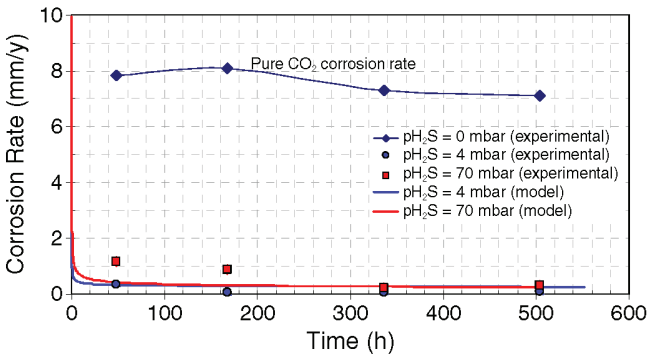

FIGURE 11. *Corrosion rate vs. time; experimental data = points, model predictions = lines; conditions: total pressure p = 3 bar, CO_2 partial pressure 2 bar, H_2S gas partial pressure from 3 mbar to 70 mbar, 70°C, experiment duration 2 days through 21 days, pH 4.2 to 4.9, liquid velocity 0.3 m/s. Experimental data taken from Singer, et al.*[34]

Figure 11, showing a marked decrease of pure CO_2 corrosion rate due to the presence of H_2S and a reasonable prediction made by the model particularly at longer exposure times. This is clearly a mixed CO_2/H_2S corrosion scenario. At a pCO_2/pH_2S ratio of 200 (pCO_2 = 2 bar, pH_2S = 4 mbar), the CO_2 contribution to the corrosion rate is 75%, with most of the balance provided by H_2S. At the pCO_2/pH_2S ratio of 28 (pCO_2 = 2 bar, pH_2S = 70 mbar), both CO_2 and H_2S account for approximately 50% of the overall corrosion rate.

Experiments by Smith and Pacheco[5]

Another study covering the same H_2S partial pressure range was published by Smith and Pacheco.[5] Three-day-long autoclave experiments were conducted at a very high total pressure (p = 138 bar) and a high CO_2 partial pressure (pCO_2 = 13.8 bar). When comparing the predictions with the experimental results of Smith and Pacheco[5] (Figure 12), it can be seen that the model underpredicts the observed rate of steel

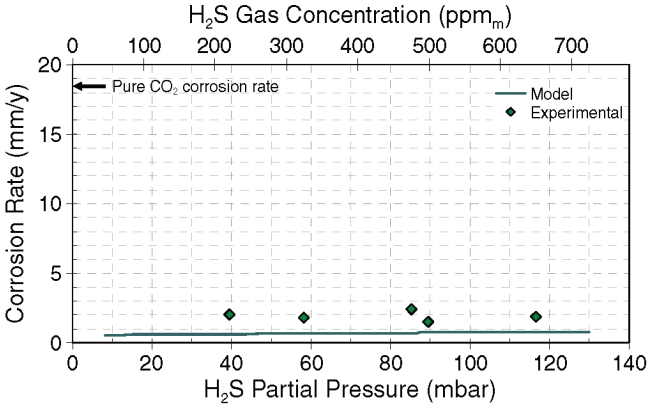

FIGURE 12. *Corrosion rate vs. H_2S partial pressure; experimental data = points, model predictions = lines; conditions: total pressure p = 137.9 bar, CO_2 partial pressure 13.8 bar, H_2S gas partial pressure from 40 mbar to 120 mbar, 50°C, experiment duration 3 days, pH 4.0 to 6.2, stagnant. Experimental data taken from Smith and Pacheco.*[5]

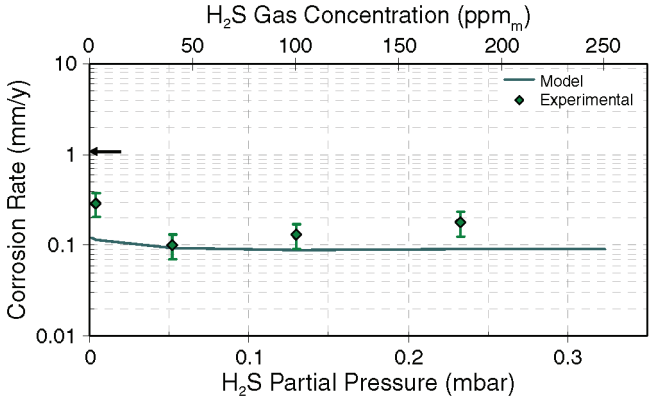

FIGURE 13. *Corrosion rate vs. partial pressure of H_2S; experimental data = points, model predictions = lines; conditions: total pressure p = 1 bar, CO_2 partial pressure 1 bar, H_2S gas partial pressure from 0.0013 mbar to 0.32 mbar, 20°C, reaction time 24 h, pH 5, 1,000 rpm. For reference: pure CO_2 corrosion rate is measured to be 1 mm/y. Data taken form Lee.[10]*

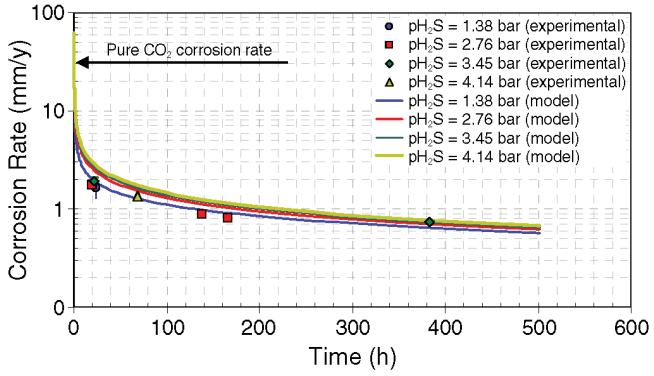

FIGURE 14. *Corrosion rate vs. time; experimental data = points, model predictions = lines; conditions: total pressure p = 7 bar, CO_2 partial pressure 6.9 bar, H_2S gas partial pressure from 1.38 bar to 4.14 bar, 120°C, experiment duration 1 day through 16 days, pH 3.95 to 4.96, liquid velocity 10 m/s. Experimental data taken from Kvarekvål, et al.[35]*

corrosion by approximately a factor of two. However, when this is compared with a pure CO_2 (H_2S-free) corrosion rate under the same conditions (which is not reported but can be predicted at almost 20 mm/y), the accuracy of the model can be considered as reasonable. At the highest pCO_2/pH_2S ratio of 3,500 (pCO_2 = 13.8 bar, pH_2S = 40 mbar) tested by Smith and Pacheco,[5] CO_2 accounts for approximately 70% of the corrosion rate and 30% can be ascribed to H_2S. At the lowest pCO_2/pH_2S ratio of 1,180 (pCO_2 = 13.8 bar, pH_2S = 116 mbar), CO_2 accounts for approximately 57% of the corrosion rate and 43% can be ascribed to H_2S.

Experiments by Lee[10]

An example of model performance at extremely low H_2S partial pressures is seen in Figure 13, where in the experiments conducted by Lee,[10] pH_2S ranged from 0.0013 mbar to 0.32 mbar, corresponding to 1 ppm_m to 250 ppm_m in the gas phase at 1 bar CO_2. Clearly, this is a CO_2-dominated corrosion scenario (pCO_2/pH_2S ratio is in the range from 10^3 to 10^6); however, again, the H_2S controls the corrosion rate. Even when present in such minute amounts, H_2S reduced the pure CO_2 (H_2S-free) corrosion rate by 3 to 10 times due to formation of a thin mackinawite film. The present model successfully captures this effect, as shown in Figure 13.

Experiments by Kvarekvål, et al.[35]

Corrosion experiments at high temperatures (120°C), high partial pressures of CO_2 (pCO_2 = 6.9 bar), and H_2S (pH_2S = 1.38 bar to 4.14 bar) were recently reported by Kvarekvål, et al.[35] In exposure lasting up to 16 days, a steadily decreasing corrosion rate was observed due to buildup of a protective iron sulfide layer (Figure 14). The effect of pH_2S increase on corrosion rate was very small and practically vanished over time. Both of these effects were readily captured by the model with very good accuracy, as seen in Figure 14. Compared to all the various experimental cases discussed above, this is the first situation where the H_2S was the dominant corrosive species. At the highest pCO_2/pH_2S ratio of 5 (pCO_2 = 6.9 bar, pH_2S = 1.38 bar), H_2S generated approximately 70% of the corrosion rate. At the lowest pCO_2/pH_2S ratio of 1.67 (pCO_2 = 6.9 bar, pH_2S = 4.14 bar), H_2S generated 82% of the overall corrosion rate.

Experiments by Bich and Goerz[36]

Another study covering corrosion of steel at high partial pressures of CO_2 (pCO_2 = 3 bar to 12.8 bar) and H_2S (pH_2S = 3 bar to 20 bar) were reported by Bich and Goerz.[36] The average corrosion rates were given for exposure lasting up to 4 days.[36] The experiments were simulated using the present H_2S model and it was found that the effect of the pH_2S increase on the final corrosion rates was very small, as shown in Figure 15. This is a situation where the H_2S was the dominant corrosive species, similar to the experiments of Kvarekvål, et al.[35] At the highest pCO_2/pH_2S ratio of 1.8 (pCO_2 = 5.3 bar, pH_2S = 3 bar), H_2S generated approximately 86% of the corrosion rate. At the lowest pCO_2/pH_2S ratio of 0.2 (pCO_2 = 4 bar, pH_2S = 20 bar), H_2S generated 97% of the overall corrosion rate. It is also noted that the model predictions show that the corrosion rate in the first reaction hour is on average 20 mm/y, with an initial corrosion rate of 60 mm/y and a final corrosion rate of 10 mm/y. Concededly, the pitting corrosion rate was reported to be 30 mm/y in a field case with similar conditions, which according to Bich and Goerz[36] is related to the very high, H_2S-driven corrosion seen at the beginning of experiments before a thick, protective, iron sulfide film forms.

Experiments by Omar, et al.[37]

H_2S corrosion data collected at the most severe experimental conditions were published recently by Omar, et al.[37] Long-term flow loop experiments (15 days to 21 days) were conducted at high partial pressure of H_2S (pH_2S = 10 bar to 30 bar), high partial pressure of CO_2 (pCO_2 = 3.3 bar to 10 bar), and low pH (2.9 to 3.2). The measured corrosion rates as a function of velocity are shown in Figure 16 for the three long-term experiments. No effect of velocity on the uniform corrosion rate could be observed in these long-term exposures, which is due to buildup of a thick, protective, sulfide layer. The model predictions also shown in Figure 16 confirm this trend and show a remarkable agreement with the experimental results in the less-extreme experiments 1 and 2 (pCO_2 = 3.3 bar; pH_2S = 10 bar), both at low (25°C) and high temperatures (80°C). In experiment no. 3, which was conducted at the most extreme set of conditions (pCO_2 = 10 bar; pH_2S = 30 bar) and high temperature (80°C), the model underpredicts the corrosion rate by a factor of 2.5. This brings us to the limitations of the model, which are discussed in the following section. In all three experiments reported by Omar, et al.,[37] the pCO_2/pH_2S ratio was about 0.3; i.e., the corrosion process and corrosion rate were dominated completely by H_2S, which contributed ≈95% of the corrosion rate.

LIMITATIONS OF THE MODEL AND FUTURE WORK

From the numerous comparisons made in the previous section, it is clear that the present mechanistic model of pure H_2S and mixed H_2S/CO_2 corrosion has performed rather well over a very broad range of conditions. The summary of all the key experimental conditions as well as the resulting experimental and predicted corrosion rates are presented in Table 1. Actually, the partial pressure of H_2S varies by 7 orders of magnitude, yet the predictions were typically within the conventional margin of error of the measurements and deviated by a factor not more than 2 to 3.[(2)] This is illustrated in Figure 17 where all the data (shown in Table 1) are presented in a parity plot in which the measured corrosion rates are compared directly with the predicted ones.

Nevertheless, the limitations of the present model need to be pointed out here, to avoid its misuse and to indicate the aspects open to improvement.

—The present model covers uniform H_2S and H_2S/CO_2 corrosion. It does not predict localized corrosion in either environment, neither does it cover pure CO_2 corrosion (H_2S-free condition). Making a link to an existing mechanistic electrochemical model of CO_2 corrosion should not be difficult. Furthermore, the present model can be considered as a solid platform for constructing an H_2S-driven localized corrosion model.

—While the present corrosion model covers a very broad range of H_2S partial pressures, it is not recommended to use this model below pH_2S = 0.01 mbar or above pH_2S = 10 bar. Similar limits apply to the CO_2 partial pressure. This leaves a very broad area of applicability for the present model.

—This model does not account for any precipitation of iron sulfide, iron carbonate, or any other

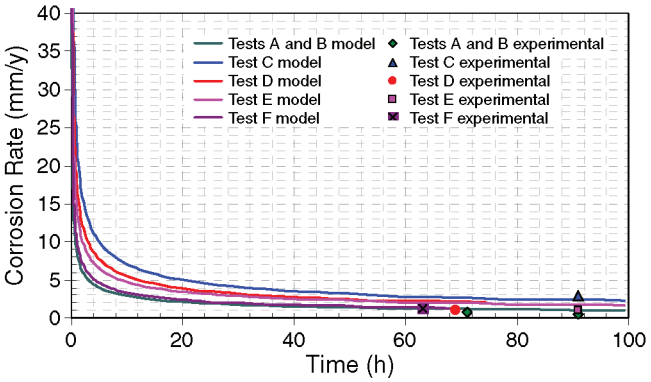

FIGURE 15. *Corrosion rate vs. time; experimental data = points, model predictions = lines; Tests A and B: p = 8.3 bar, pCO_2 = 5.3 bar, pH_2S = 3 bar, 60°C, (A) 71 h and (B) 91 h; Test C: p = 24 bar, pCO_2 = 4 bar, pH_2S = 20 bar, 70°C, 91 h; Test D: p = 15.7 bar, pCO_2 = 3.5 bar, pH_2S = 12.2 bar, 65°C, 69 h; Test E: p = 20.8 bar, pCO_2 = 12.8 bar, pH_2S = 8 bar, 65°C, 91 h; Test F: p = 7.2 bar, pCO_2 = 3 bar, pH_2S = 4.2 bar, 65°C, 63 h; experimental data taken from Bich and Goerz.*[36]

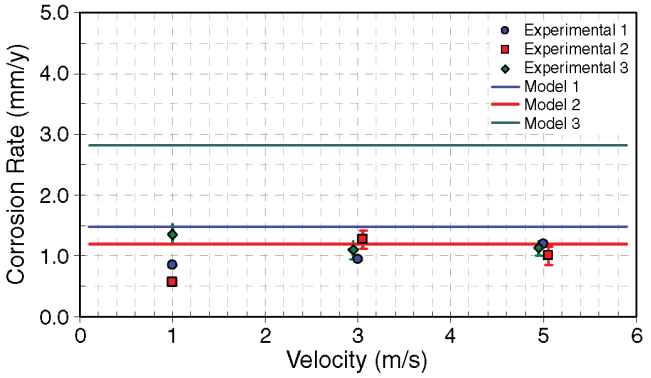

FIGURE 16. *Corrosion rate vs. velocity; experimental data = points, model predictions = lines; Exp. 1.: 19 days, p = 40 bar, pCO_2 = 3.3 bar, pH_2S = 10 bar, 80°C, pH 3.1, v = 1 m/s to 5 m/s; Exp. 2.: 21 days, p = 40 bar, pCO_2 = 3.3 bar, pH_2S = 10 bar, 25°C, pH 3.2, v = 1 m/s to 5 m/s; Exp. 3.: 10 days, p = 40 bar, pCO_2 = 10 bar, pH_2S = 30 bar, 80°C, pH 2.9, v = 1 m/s to 5 m/s; experimental data taken from Omar, et al.*[37]

[(2)] When interpreting graphs such as the one shown in Figure 17, one should keep in mind that the various experimental data points always have a measurement error associated with them (not shown in Figure 17 for clarity reasons); i.e., the data collected in various experiments are not in perfect agreement with each other. Therefore, one has to account for this when comparing the experimental data with numerical predictions, which carry their own uncertainty (also not shown in Figure 17).

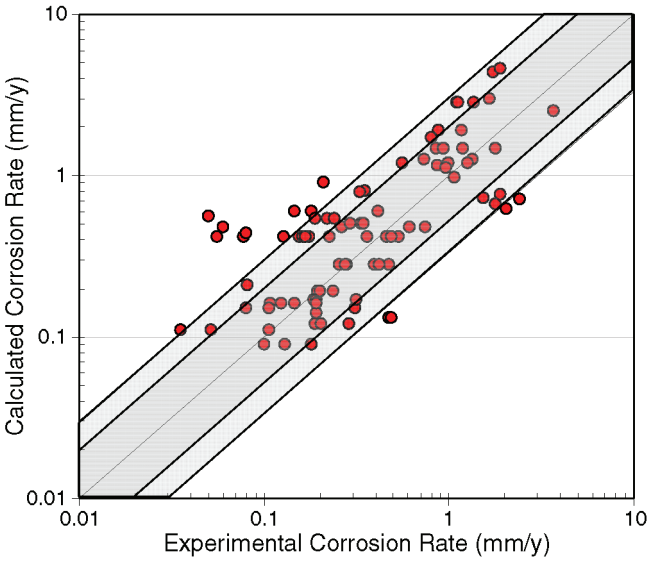

FIGURE 17. *Predicted vs. experimental corrosion rates taken from a wide variety of studies,[5,10,33-37] covering a very broad range of parameters: p = 1 bar to 140 bar, 20°C to 120°C, pCO_2 = 0 bar to 13.8 bar, $pH_2S = 1.3 \times 10^{-6}$ to 30 bar, pH 3.1 to 6.6, v = 0 to 10 m/s. The wider outer pair of lines outlines an area that is within a factor of 3 compared to a "perfect" match (given by the diagonal line). The narrower, inner pair of lines outlines an area that is within a factor 2.*

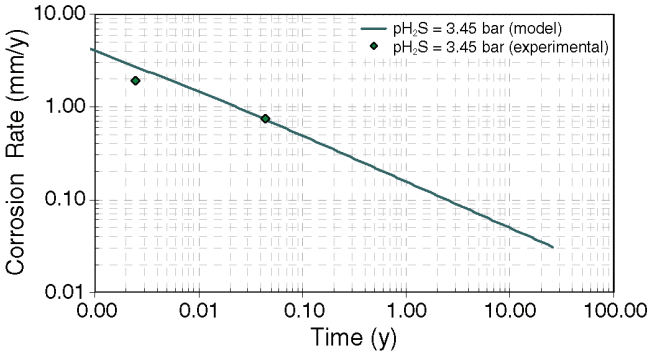

FIGURE 18. *Extension of corrosion prediction to a 25-year lifetime; experimental (points), predicted (lines); conditions: CO_2 partial pressure 6.9 bar, H_2S partial pressure 3.45 bar, 120°C, pH 4, liquid velocity 10 m/s; taken from Kvarekvål, et al.[35]*

scale; therefore, in cases where this is deemed important for corrosion, the model should be used with caution. The model also does not account for various transformations of sulfide layer from one type to another, which are known to happen over time. However, the present model is mechanistic and transient and therefore new physics that covers kinetics of precipitation and sulfide transformations can be added easily to it.

—The present model does not account for dissolution of the sulfide layer that may occur at very low pH. Therefore, the use of this model at pH < 3 is not recommended. Similarly, the model should be used with caution for pH > 7 where it has not been tested. Again, due to its mechanistic nature, extensions of the present model to cover these new phenomena are not prohibitively difficult to implement and are already being developed.

—The model in its present state does not cover the effect of organic acids on mixed H_2S and H_2S/CO_2 corrosion; therefore, it should not be used when organic acids are present in the system. A practical threshold for the validity of the present model is: <1 ppm of organic acids in the brine. This effect is now being modeled and implemented in the latest versions of the model.

—The model does not account for the effect of high chloride concentrations, oxygen, elemental sulfur, or any other unspecified condition that is known to affect the corrosion rate and is not explicitly covered in the theoretical underpinnings of the present model.

Finally, it is worthwhile commenting on the fact that even the longest H_2S-containing corrosion experiments, which are practically achievable in the lab, are of the order of a few weeks or at best a few months, while predictions are meant to cover a period of at least a few decades to be meaningful. With this in mind, it is interesting to take one of the conditions simulated in the previous sections and extrapolate the prediction over such a long lifetime. One of the experimental conditions used by Kvarekvål, et al.,[35] was used here (pCO_2 = 6.9 bar, pH_2S = 3.45 bar, T = 120°C, pH 4, v = 10 m/s) and the simulation was extended to 25 years. The result is shown in Figure 18. The corrosion rate was predicted to start out rather high as observed in the experiments; however, it was reduced to below 0.1 mm/y after 2 years and was as low as 0.03 mm/y after 25 years. The average corrosion rate over this period was only 0.06 mm/y, which amounts to a wall thickness loss of only 1.5 mm over the 25 years, an acceptable amount by any practical account. Actually, most of the other conditions simulated have shown that rather low H_2S uniform corrosion rates are obtained for very long exposures, which agrees with general field experience as recently discussed by Bonis, et al.[7] Nevertheless, no quantitative long-term lab data are currently available to back up these long-term predictions.

CONCLUSIONS

❖ The corrosion rate of mild steel in H_2S and CO_2/H_2S corrosion is affected mainly by H_2S concentration, temperature, velocity, and the protectiveness of the sulfide layer. CO_2 partial pressure and pH have an effect on the corrosion rate at very low H_2S concentrations.

❖ The amount of iron sulfide layer retained on the steel surface depends on the layer formation rate and

the layer damage rate. The layer forms directly by corrosion and/or by precipitation. The layer damage can occur by mechanical and/or chemical means.

❖ A rather simple mechanistic model of H_2S and H_2S/CO_2 corrosion is developed to accurately predict the corrosion rate.

❖ The model has been verified extensively with a broad database where the partial pressure of H_2S spans 7 orders of magnitude and includes CO_2.

❖ The current version of the model does not yet include iron sulfide precipitation effects, nor hydrodynamic effects on film damage, which will be addressed in future work.

ACKNOWLEDGMENTS

During this work, W. Sun was supported by the Ohio University Donald Clippinger Fellowship. A part of the experiments referred to in this paper were conducted at CANMET Materials Technology Laboratory, Natural Resources Canada, and the authors thank S. Papavinasam for his help. We are also indebted to D. Young for many useful comments and advice on the structure and properties of various iron sulfides. The authors would like to acknowledge the companies who provided the financial support and technical guidance for this project. They are Baker Petrolite, BP, Champion Technologies, Chevron, Clariant, Columbia Gas Transmission, ConocoPhillips, ENI, ExxonMobil, MI SWACO, Nalco, Oxy, PETRONAS, PETROBRAS, PTTEP, Saudi Aramco, Shell, Total, and Tenaris.

REFERENCES

1. D.W. Shoesmith, P. Taylor, M.G. Bailey, D.G. Owen, *J. Electrochem. Soc.* 125 (1980): p. 1,007-1,015.
2. D.W. Shoesmith, "Formation, Transformation, and Dissolution of Phases Formed on Surfaces," Lash Miller Award Address, Electrochemical Society Meeting, held Nov. 27 (Ottawa, 1981).
3. S.N. Smith, "A Proposed Mechanism for Corrosion in Slightly Sour Oil and Gas Production," 12th Int. Corros. Cong., paper no. 385, held September 19-24 (Houston, TX, 1993).
4. S.N. Smith, E.J. Wright, "Prediction of Minimum H_2S Levels Required for Slightly Sour Corrosion," CORROSION/94, paper no. 11 (Houston, TX: NACE International, 1994).
5. S.N. Smith, J.L. Pacheco, "Prediction of Corrosion in Slightly Sour Environments," CORROSION/2002, paper no. 02241 (Houston, TX: NACE, 2002).
6. S.N. Smith, M. Joosten, "Corrosion of Carbon Steel by H_2S in CO_2-Containing Oilfield Environments," CORROSION/2006, paper no. 06115 (Houston, TX: NACE, 2006).
7. M. Bonis, M. Girgis, K. Goerz, R. MacDonald, "Weight Loss Corrosion with H_2S: Using Past Operations for Designing Future Facilities," CORROSION/2006, paper no. 06122 (Houston, TX: NACE, 2006).
8. W. Sun, S. Nešić, *Corrosion* 64, 4 (2008): p. 334.
9. W. Sun, S. Nešić, S. Papavinasam, *Corrosion* 64, 7 (2008): p. 586.
10. K.J. Lee, "A Mechanistic Modeling of CO_2 Corrosion of Mild Steel in the Presence of H_2S" (Ph.D. diss., Ohio University, 2004).
11. F.H. Meyer, O.L. Riggs, R.L. McGlasson, J.D. Sudbury, *Corrosion* 14 (1958): p. 109.
12. L.G. Benning, R.T. Wilkin, H.L. Barnes, *Chem. Geol.* 167 (2000): p. 25.
13. A. Anderko, P.J. Shuler, *Comput. Geosci.* 23 (1997): p. 647.
14. A. Anderko, P.J. Shuler, "Modeling the Formation of Iron Sulfide Layers Using Thermodynamic Simulation," CORROSION/98, paper no. 64 (Houston, TX: NACE, 1998).
15. A. Anderko, R.D. Young, "Simulation of CO_2/H_2S Corrosion Using Thermodynamic and Electrochemical Models," CORROSION/99, paper no. 31 (Houston, TX: NACE, 1999).
16. A. Anderko, "Simulation of $FeCO_3$/FeS Layer Formation Using Thermodynamic and Electrochemical Models," CORROSION/2000, paper no. 102 (Houston, TX: NACE, 2000).
17. P. Taylor, *Am. Mineral.* 65 (1980): p. 1,026-1,030.
18. P. Marcus, E. Protopopoff, *J. Electrochem. Soc.* 137 (1990): p. 2,709.
19. J.S. Smith, J.D.A. Miller, *Br. Corros. J.* 10 (1975): p. 136-143.
20. W. Sun, S. Nešić, S. Papavinasam, "Kinetics of Iron Sulfide and Mixed Iron Sulfide/Carbonate Scale Precipitation in CO_2/H_2S Corrosion," CORROSION/2006, paper no. 06644 (Houston, TX: NACE, 2006).
21. K.-L.J. Lee, S. Nešić, "EIS Investigation on the Electrochemistry of CO_2/H_2S Corrosion," CORROSION/2004, paper no. 04728 (Houston, TX: NACE, 2004).
22. S. Nešić, J. Postlethwaite, S. Olsen, *Corrosion* 52 (1996): p. 280-294.
23. M. Nordsveen, S. Nešić, R. Nyborg, A. Stangeland, *Corros. Sci.* 59 (2003): p. 443-457.
24. S. Nešić, K.-L.J. Lee, *Corros. Sci.* 59 (2003): p. 616-628.
25. M. Schulte, M. Schutz, *Oxid. Met.* 51 (1999): p. 55-77.
26. A. Dravnieks, C.H. Samans, *J. Electrochem. Soc.* 105 (1958): p. 183-191.
27. D.N. Tsipas, H. Noguera, J. Rus, *Mater. Chem. Phys.* 18 (1987): p. 295-303.
28. B. Brown, S. Nešić, S.R. Parakala, "CO_2 Corrosion in the Presence of Trace Amounts of H_2S," CORROSION/2004, paper no. 04736 (Houston, TX: NACE, 2004).
29. M. Schutze, *Protective Oxide Layers and Their Breakdown* (Chichester, U.K.: John Wiley and Sons, 1997).
30. B. Brown, S. Nešić, "H_2S/CO_2 Corrosion in Multiphase Flow," Ohio University Advisory Board Meeting Report, internal report, 2006.
31. S. Nešić, B.F.M. Pots, J. Postlethwaite, N. Thevenot, *J. Corros. Sci. Eng.* (1995), ISSN 1466-8858.
32. J. Oddo, M. Tomson, "Simplified Calculation of $CaCO_3$ Saturation at High Temperatures and Pressures in Brine Solutions," SPE of AIME (Richardson, TX: Society of Petroleum Engineers, 1982), p. 1,583-1,590.
33. W. Sun, "Kinetics of Iron Carbonate and Iron Sulfide Layer Formation in CO_2/H_2S Corrosion" (Ph.D. diss., Ohio University, 2006).
34. M. Singer, B. Brown, A. Camacho, S. Nešić, "Combined Effect of CO_2, H_2S, and Acetic Acid on Bottom-of-the-Line Corrosion," CORROSION/2007, paper no. 07661 (Houston, TX: NACE, 2007).
35. J. Kvarekvål, R. Nyborg, H. Choi, "Formation of Multilayer Iron Sulfide Films During High-Temperature CO_2/H_2S Corrosion of Carbon Steel," CORROSION/2003, paper no. 03339 (Houston, TX: NACE, 2003).
36. N.N. Bich, K. Goerz, "Caroline Pipeline Failure: Findings on Corrosion Mechanisms in Wet Sour Gas Systems Containing Significant CO_2," CORROSION/96, paper no. 26 (Houston, TX: NACE, 1996).
37. I.H. Omar, Y.M. Gunaltun, J. Kvarekvål, A. Dugstad, "H_2S Corrosion of Carbon Steel Under Simulated Kashagan Field Conditions," CORROSION/2005, paper no. 05300 (Houston, TX: NACE, 2005).